Relativistic close-coupling calculations for photoionization and recombination of Ne-like Fe XVII

Hong Lin Zhang
Applied Theoretical and Computational Physics Division, Los Alamos National Laboratory, Los Alamos, New Mexico 87545

Sultana N. Nahar and Anil K. Pradhan
Department of Astronomy, The Ohio State University, Columbus, Ohio 43210

(Received 1 March 2001; published 20 August 2001)

Relativistic and channel coupling effects in photoionization and unified electronic recombination of Fe XVII are demonstrated with an extensive 60-level close-coupling calculation using the Breit-Pauli *R*-matrix method. A multiconfiguration eigenfunction expansion up to the $n=3$ levels of the core ion Fe XVIII is employed with five spectroscopic configurations $2s^22p^5, 2s2p^6, 2s^22p^4\,3s, 3p, 3d$, and a number of correlation configurations. The unified $e+$ion recombination calculations for $e+$Fe XVIII$\rightarrow$Fe XVII include both the nonresonant and resonant recombination (''radiative'' and ''dielectronic recombination''—RR and DR). Photoionization and $e+$ion recombination calculations are carried out for the total and the level-specific cross sections, including the ground and several hundred excited bound levels of Fe XVII (up to fine-structure levels with $n=10$). The low-energy and the high-energy cross sections are compared from (i) a three-level calculation including only the $2s^2p^5$ ($^2P^o_{1/2,3/2}$) and $2s2p^6$ ($^2S_{1/2}$) levels of Fe XVIII, and (ii) the first 60-level calculation with $\Delta n>0$ coupled channels. Strong channel coupling effects are demonstrated throughout the energy ranges considered, in particular via giant photoexcitation-of-core (PEC) resonances due to *L-M* shell dipole transition arrays $2p^5\rightarrow 2p^4\,3s, 3d$ in Fe XIII that enhance effective cross sections by orders of magnitude. Comparison is made with previous theoretical and experimental works on photoionization and recombination that considered the relatively small low-energy region (i), and the weaker $\Delta n=0$ couplings. While the simpler three-level results describe the near-threshold photoionization and recombination, they are inadequate for practical applications that also require the higher-energy cross sections for modeling ionization balance of Fe XVII in laboratory and astrophysical plasmas. The present 60-level results should provide reasonably complete and accurate datasets for both photoionization and $e+$ion recombination of Fe XVII.

DOI: 10.1103/PhysRevA.64.032719 PACS number(s): 34.80.Kw, 32.80.Dz, 32.80.Fb

I. INTRODUCTION

Laboratory, astrophysical, and theoretical studies of Fe XVII are of considerable interest as it is a prime constituent in high-temperature plasmas responsible for strong x-ray emission [1–3]. A number of atomic processes need to be considered in detail, primarily electron-impact excitation, photoionization, $e+$ion recombination, and radiative transitions. Large-scale atomic calculations are in progress for all of these processes in Fe XVII under the Iron Project and related works [4–6], in extended energy ranges suitable for practical applications. While electron-impact excitation is an independent part of this effort, in this work we describe photoionization and the $e+$ion recombination of Fe XVII. The coupled channel approximation, including relativistic effects for many channel systems, can be very involved owing to many infinite series of resonance structures converging on to the various excited levels of the core ion. Whereas the relativistic and coupling effects have been studied previously, all such theoretical and experimental studies of Fe XVII photoionization (e.g., Haque *et al.* [7] and Mohan *et al.* [3]) have been limited to the ground state and the relatively small energy range spanned by core excitations within the $n=2$ complex of the residual ion Fe XVIII comprised of three fine-structure levels up to about 132 eV, i.e.,

$$h\nu+\text{Fe XVII}\ (2s^22p^6\,{}^1S_0)\rightarrow e+\text{Fe XVIII}\ (2s^22p^5\,{}^2P^o_{3/2,1/2}), 2s2p^6({}^2S_{1/2}). \quad (1.1)$$

Although the near-threshold behavior of photoionization and recombination cross sections (Pradhan *et al.* [8]) is physically interesting, it is inadequate for practical applications that require the cross sections to be calculated up to high energies typical of the variety of conditions where *L*-shell ions are abundant. Purely photoionized plasmas, such as in H II regions, planetary nebulas, novas, etc., are typically low temperature, while the coronal plasmas cover a much wider range [9]. For example, the temperature of maximum abundance of Fe XVII in the coronal ionization equilibrium is about 4×10^6 K [10]. Furthermore, in astrophysical objects such as the warm absorber ionized gas thought to surround the central black hole in active galactic nuclei, the plasma is most likely to be of a composite nature since most ionization states of several elements are observed (e.g., [1]). High accuracy throughout the energy range of practical importance is therefore essential.

As the $e+$ion recombination is unified in nature, it is theoretically desirable to consider the nonresonant and resonant processes [radiative recombination (RR) and dielectric recombination (DR)] together. A unified theoretical formulation has been developed [11,13], including relativistic fine structure [14], and used to compute cross sections and rates for many atomic systems, such as the *K*-shell systems C IV–C V and Fe XXIV–Fe XXV of interest in x-ray spectroscopy [15,16]. The unified results may be directly compared with experimental results, without the need to separate RR

TABLE I. Fine-structure energy levels for the 60CC eigenfunction expansion of the target ion Fe XVIII compared to the NIST [22]. The level energies are in rydbergs.

i	Configuration	Term	$2J$	E (Present)	E (NIST)	i	Configuration	Term	$2J$	E (Present)	E (NIST)
1	$2s^2 2p^5$	^2P	3	0.00000	0.	31	$2s^2 2p^4 3d$	^4D	5	62.299	
2		^2P	1	0.94212	0.93477	32		^4D	7	62.311	
3	$2s2p^6$	^2S	1	9.80691	9.70228	33		^4D	1	62.429	62.906
4	$2s^2 2p^4 3s$	^4P	5	56.991	56.690	34		^4D	3	62.341	63.050
5		^2P	3	57.239	56.936	35	$2s^2 2p^4 3p$	^2P	3	62.461	
6		^4P	1	57.671	57.502	36	$2s^2 2p^4 3d$	^4F	9	62.535	
7		^4P	3	57.836	57.572	37		^2F	7	62.629	
8		^2P	1	58.068	57.798	38	$2s^2 2p^4 3p$	^2P	1	62.686	
9		^2D	5	58.609	58.000	39	$2s^2 2p^4 3d$	^4P	1	62.767	62.496
10		^2D	3	58.642	58.355	40		^4P	3	62.905	62.625
11	$2s^2 2p^4 3p$	^4P	3	59.209		41		^4F	5	62.985	
12		^4P	5	59.238		42		^2P	1	63.123	
13		^4P	1	59.478		43		^4F	3	63.156	
14		^4D	7	59.525		44		^2F	5	63.177	62.698
15		^2D	5	59.542		45		^4F	7	63.271	
16	$2s^2 2p^4 3s$	^2S	1	59.947	59.916	46		^2D	3	63.302	
17	$2s^2 2p^4 3p$	^2P	1	59.982		47		^4P	5	63.451	62.911
18		^4D	3	60.005		48		^2P	3	63.574	63.308
19		^4D	1	60.012		49		^2D	5	63.672	63.390
20		^2D	3	60.147		50		^2G	7	63.945	
21		^4D	5	60.281		51		^2G	9	63.981	
22		^2P	3	60.320		52		^2S	1	64.198	63.919
23		^2S	1	60.465		53		^2F	5	64.200	
24		^4S	3	60.510		54		^2F	7	64.301	
25		^2F	5	60.851		55		^2P	3	64.432	64.138
26		^2F	7	61.028		56		^2D	5	64.488	64.160
27		^2D	3	61.165		57		^2D	3	64.703	64.391
28		^2D	5	61.272		58		^2P	1	64.767	64.464
29		^2P	3	61.761		59		^2D	5	65.481	65.305
30		^2P	1	61.899		60		^2D	3	65.669	65.468

and DR. In this paper we present details of the low-energy results for Fe XVII and show that not only are the unified cross sections and rates in good agreement with experiment, but they also illustrate how the unified calculations avoid the basic inconsistency and incompleteness of photoionization and recombination data for the modeling of laboratory and astrophysical plasma sources.

The present paper describes in detail the three-level and the 60-level close-coupling calculations, with a discussion of the relativistic and coupling effects and comparison with earlier three-level theoretical and experimental data for photoionization and recombination. While photoionization and recombination are usually considered separately, we exemplify and emphasize the underlying physical unity, via detailed balance, between the two processes as naturally treated in the close-coupling method.

II. THEORY

Photoionization and $e+$ion recombination may both be considered using *identical* coupled channel wave-function expansion,

$$\Psi(E)=A\sum_i \chi_i\theta_i+\sum_j c_j\Phi_j, \tag{2.1}$$

where Ψ represents an $(N+1)$-electron bound or continuum state, depending on $E<0$ or $E>0$, expressed in terms of the N-electron residual core-ion eigenfunctions. The χ_i is the target wave function in a specific state $S_iL_i\pi_i$ or $J_i\pi_i$, and θ_i is the wave function for the $(N+1)$th electron in a channel labeled as $S_iL_i(J_i)\pi_i k_i^2 l_i(SL\pi$ or $J\pi)$, k_i^2 being its incident kinetic energy. Φ_j's are the correlation functions of the $(N+1)$-electron system that account for short-range correlation and the orthogonality between the continuum and the bound orbitals. The R-matrix method [17,18], and its relativistic Breit-Pauli extension [19], enables a solution for the total Ψ, with a suitable expansion over the χ_i. The Breit-Pauli R-matrix (BPRM) method has been extensively employed for electron-impact excitation under the Iron Project [4,20]. The extension of the BPRM formulation to unified electronic recombination [13,16] and theoretically self-consistent calculations of photoionization and recombination is sketched below.

TABLE II. Comparison of the present dipole oscillator strengths (the gf values) for fine-structure transitions in Fe XVIII with the compiled NIST [23] data. See Table I for the level index.

i	j	NIST	Present
1	3	0.242	0.222
1	4	0.021	0.018
1	6	0.015	0.012
1	8	0.104	0.079
1	9	0.242	0.191
1	16	0.019	0.014
1	43	0.096	0.085
1	52	0.975	0.879
1	55	2.300	2.344
1	57	0.516	0.511
1	59	0.193	0.190
1	60	0.011	0.008
2	3	0.107	0.100
2	8	0.116	0.095
2	10	0.196	0.167
2	16	0.079	0.055
2	52	0.169	0.159
2	55	0.399	0.373
2	57	1.855	1.579
2	60	1.794	1.831

The recombination of an incoming electron to the target ion may occur through nonresonant, background continuum, usually referred to as radiative recombination (RR),

$$e+X^{2+}\rightarrow h\nu+X^{+}, \tag{2.2}$$

which is the inverse process of direct photoionization, or through the two-step recombination process via autoionizing resonances, i.e., dielectronic recombination (DR),

$$e+X^{++}\rightarrow (X^{+})^{**}\rightarrow \begin{cases} e+X^{2+} \\ h\nu+X^{+}, \end{cases} \tag{2.3}$$

where the incident electron is in a quasibound doubly excited state which leads either to (i) autoionization, a radiationless transition to a lower state of the ion and the free electron, or to (ii) radiative stabilization predominantly via decay of the ion core, usually to the ground state, and the bound electron.

In the unified treatment the photoionization cross sections $\sigma_{\rm PI}$ of a large number of low-n bound states—all possible states with $n\leqslant n_{\rm max}\sim 10$—are obtained in the close coupling (CC) approximation as in the Opacity Project [5]. Coupled channel calculations for $\sigma_{\rm PI}$ include both the background and the resonance structures (due to the doubly excited autoionizing states) in the cross sections. The recombination cross section $\sigma_{\rm RC}$ is related to $\sigma_{\rm PI}$ through detailed balance (Milne relation) as

$$\sigma_{\rm RC}(\epsilon)=\frac{\alpha^2}{4}\frac{g_i}{g_j}\frac{(\epsilon+I)^2}{\epsilon}\sigma_{\rm PI} \tag{2.4}$$

in Rydberg units; α is the fine-structure constant, ϵ is the photoelectron energy, and I is the ionization potential.

Resonant and nonresonant electronic recombination takes place into an infinite number of bound levels of the $e+$ion system. These are divided into two groups: (a) the low-n ($n\leqslant n_o\approx 10$) levels, considered via detailed close-coupling calculations for photorecombination, with highly resolved delineation of autoionizing resonances, and (b) the high-n ($n_o\leqslant n\leqslant\infty$) recombining levels via DR, neglecting the background. In previous works (e.g., [13]) it has been shown that in the energy region corresponding to (b), below threshold for DR, the nonresonant contribution is negligible. The DR cross sections converge on to the electron-impact excitation cross section at threshold ($n\rightarrow\infty$), as required by unitarity, i.e., conservation of photon and electron fluxes. This theoretical limit is an important check on the calculations, and enables a determination of field ionization of Rydberg levels of resonances contributing to DR.

The *ab initio* method outlined above is a theoretically and computationally unified treatment based on the close-coupling approximation. Recombination involves an infinite number of recombined bound states, and several infinite series of resonances. In principle, the unified method may be used for photoionization and/or photorecombination of arbitrarily high n,l,J levels. However, in practice approximations may be made for sufficiently high quantum numbers. Background recombination is negligible, and DR dominates, usually for $n_{max}\geqslant 10$. Similarly, background (nonresonant) cross sections may be accurately obtained using hydrogenic approximation for n,l levels with $n>10$. But there is nothing particular about $n_{max}=10$, and any larger or lower value may be used provided the approximations are verifiably valid, as has been shown in our previous works and is done in the present calculations. For example, $n=(18-22)+$resonances in the present work are fully delineated using group (a) photorecombination calculations, and not DR. Thus the use of these approximations does not result in any significant error, or loss of generality, and does not detract from the main part of the calculations that are a unified representation of the nonresonant and resonant recombination (RR and DR), including any interference effects between the two. The present DR calculations use an extension of the precise theory by Bell and Seaton [12], based on multichannel quantum defect theory, that is very accurate for high n (correspondence between photorecombination and DR is established in our previous work [13]). Finally, all close-coupling scattering and photoionization calculations employ a ''top-up'' procedure for high partial waves, and approximations for high-n resonances below Rydberg series limits as $n\rightarrow\infty$ (e.g., ''Gailitis averaging''). Such procedures are routinely implemented in large-scale calculations in the Opacity Project ([5] and references therein) and the Iron Project R-matrix calculations ([6]) that the unified method for $e+$ion recombination is based upon.

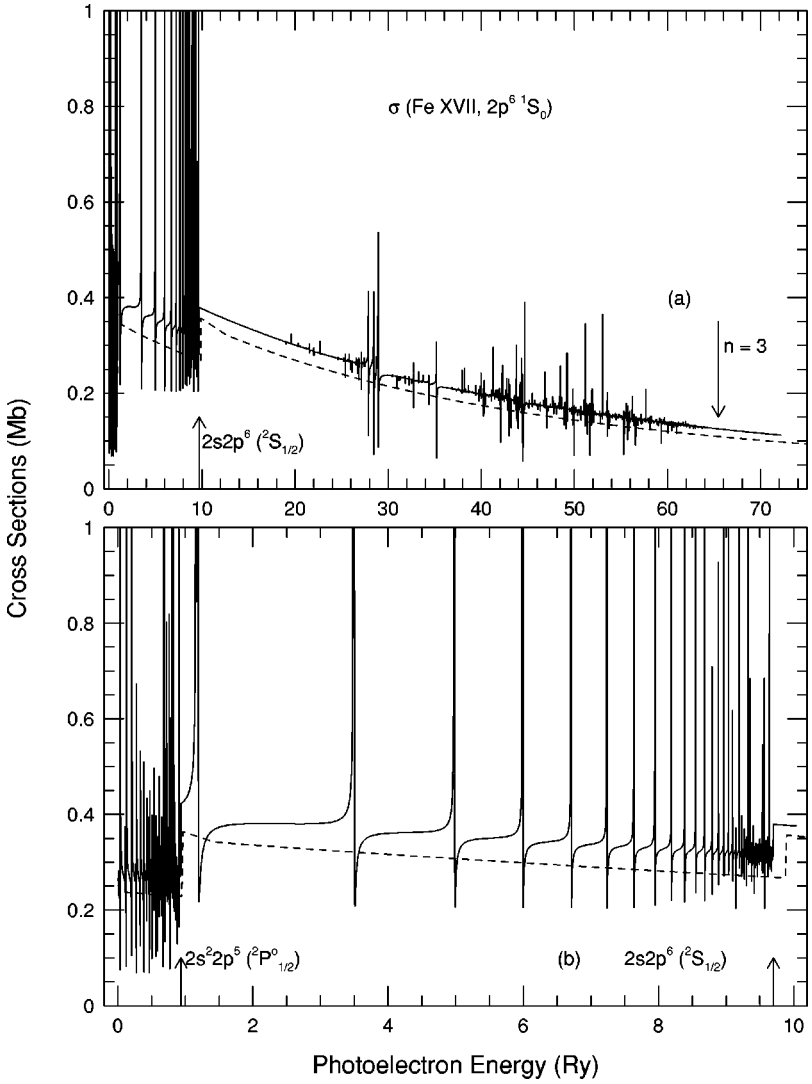

FIG. 1. Photoionization cross section of the Fe XVII ground state $2s^2 2p^6(^1S_0)$: (a) up to and above the $n=3$ thresholds of the core-ion Fe XVIII, 60-level close-coupling (60CC); (b) expanded view up to the $n=2$ thresholds $2s^2 2p^5(^2P^o_{3/2,1/2})$ and $2s2p^6(^2S_{1/2})$. The dashed lines are results from the relativistic distorted wave calculations [24].

III. COMPUTATIONS

The complete wave-function expansion entails the 60 fine-structure levels of Fe XVIII given in Table I. These are obtained from an optimized configuration-interaction- (CI) type calculation using the code SUPERSTRUCTURE [21]. The configuration set is divided into the five *spectroscopic* configurations $2s^2 2p^5, 2s2p^6, 2s^2 2p^4\, 3s, 3p, 3d$ that dominate the 60 core-level wave functions, and *correlation* configurations, $2s2p^5\, 3s, 3p, 3d; 2p^6\, 3s, 3p, 3d$. Calculated Fe XVIII eigenenergies are compared with experimental data from the National Institute for Standards and Technology (NIST [22]). The accuracy of the eigenfunctions is also ascertained by comparing the Fe XVIII oscillator strengths for dipole transitions with available data from NIST [23] in Table II. Photoionization and recombination calculations both employ the Fe XVIII eigenfunctions with the same CI. We carry out two sets of calculations, (i) a three-level calculation including only the $n=2$ levels, and (ii) the 60-level eigenfunction expansion including most of the $n=3$ complex. The inner $2s$-shell excitations are not considered owing to computational constraints and possibly weaker couplings (only the allowed $2s$-$3p$ core excitations are likely to be of importance, and not the $2s$-$3s$ or $2s$-$3d$).

For the three-level case, since we calculate both photoionization and photorecombination cross sections, we include many $LS\pi$ symmetries to obtain 15 total $J\pi$ symmetries. Specifically these are $J=0-7$ for the even parity and $J=0-6$ for the odd parity, and the $LS\pi$ symmetries used are $L=0-8$ for both singlets and triplets in both parities. For the 60-level case, presently we only calculate photoionization cross section for the ground level and some selected excited levels. Therefore, we only include $J=0$ for the even (0^e) and $J=1$ for the odd parity (1^o) at this moment. All the $LS\pi$ symmetries that contribute to these two $LS\pi$'s are included. Of course, for obtaining photorecombination cross sections we need to include an many $J\pi$ symmetries as in the three-level case.

IV. RESULTS AND DISCUSSION

The following sections present a sample of the extensive results from the two sets of calculations for photoionization and $e+$ion recombination. The three-level calculations are

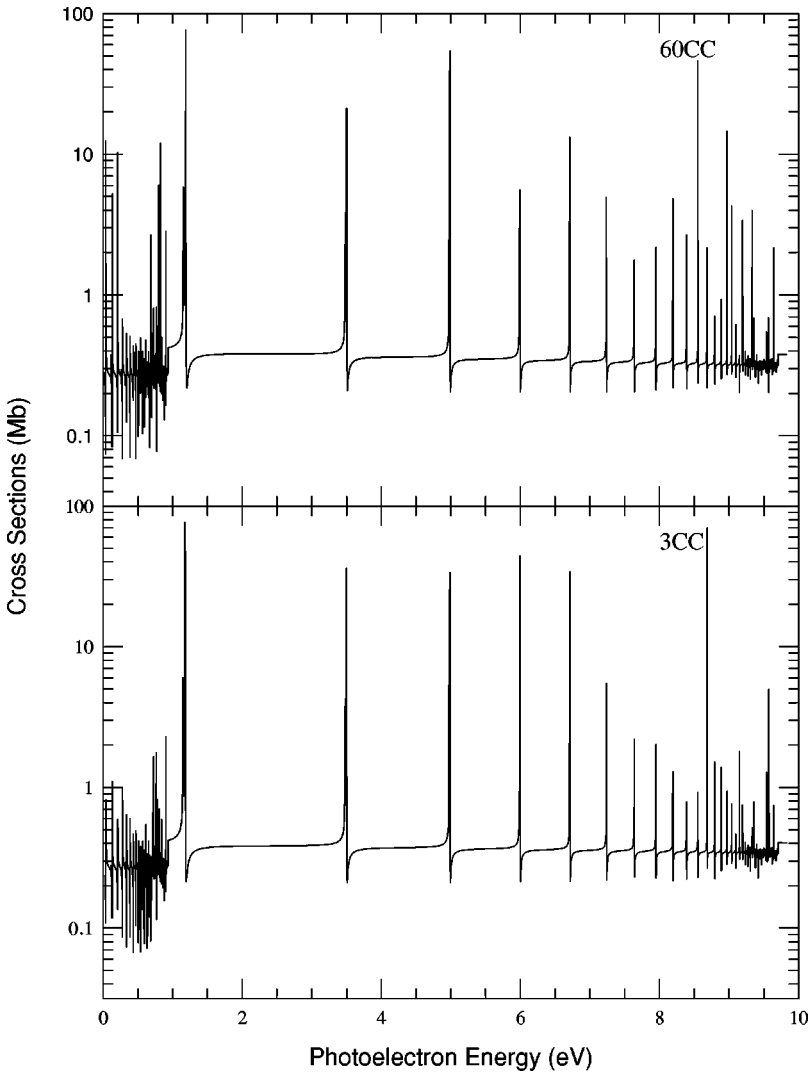

FIG. 2. The 60CC and the 3CC cross sections in the region below the Fe XVIII $2s2p^6\,{}^2S_{1/2}$ threshold. Although there is no significant coupling effect below the $n=2$ threshold, the $n=3$ thresholds are strongly coupled above the $n=2$ levels (e.g., Fig. 3).

compared with earlier theoretical and experimental works. The present close-coupling calculations for the three-level and the 60-level cases are labeled 3CC and 60CC, respectively.

A. Photoionization

Figure 1(a) presents the BPRM photoionization cross section for the ground level $2s^22p^6(^1S_0)$ of Fe XVII from the 60CC calculation (solid line), showing the series of resonances converging on to the $n=2$ thresholds $2s^22p^5(^2P^o_{1/2})$, $2s2p^6(^2S_{1/2})$, and the $n=3$ thresholds. For comparison, the nonresonant cross sections from a relativistic distorted wave (RDW) calculation (e.g., [24]) are also shown (dashed line). The resonance pattern, and the background cross sections, are essentially similar to the three-level calculations in [3,7] in the relativistic random-phase approximation (RRPA), with resonances included using multichannel quantum defect theory (MQDT), and the *LS* and Breit-Pauli *JK*-coupled *R*-matrix calculations also reported by Haque *et al.* [7]. While there are no significant differences in magnitude or detail with the earlier calculations, it might be noted that the near-threshold region spanning the three levels of the $n=2$ complex is rather simple in terms of structure and coupling effects. Figure 1(b) shows an expanded view of this region with series of resonances $2s^22p^5(^2P^o_{1/2})nl$ and the stronger series, connected to the ground level via a dipole core transition, $2s2p^6(^2S_{1/2})nl$. Figure 2 shows a comparison between the 60CC and the 3CC calculations, with similar resolution, indicating that below the $n=2$ thresholds there is no significant difference between the two.

1. Channel coupling effects

The situation is considerably more complicated above the $n=2$ complex. Although the ground-level photoionization cross section of Fe XVII is not hugely affected by the $n=3$ complexes of resonances [Fig. 1(a)], the excited level cross sections are, as seen in Figs. 3(a)–3(c). This is of considerable importance in $e+$ion recombination work where photorecombination to group (a) levels is considered explicitly. The dense and detailed resonance structures converging on to the 57 $n=3$ levels, and in between, would enhance the effective photoionization and recombination cross sections and rates far above the background. It might be noted that the resonances in cross sections below the $n=2$, in the energy

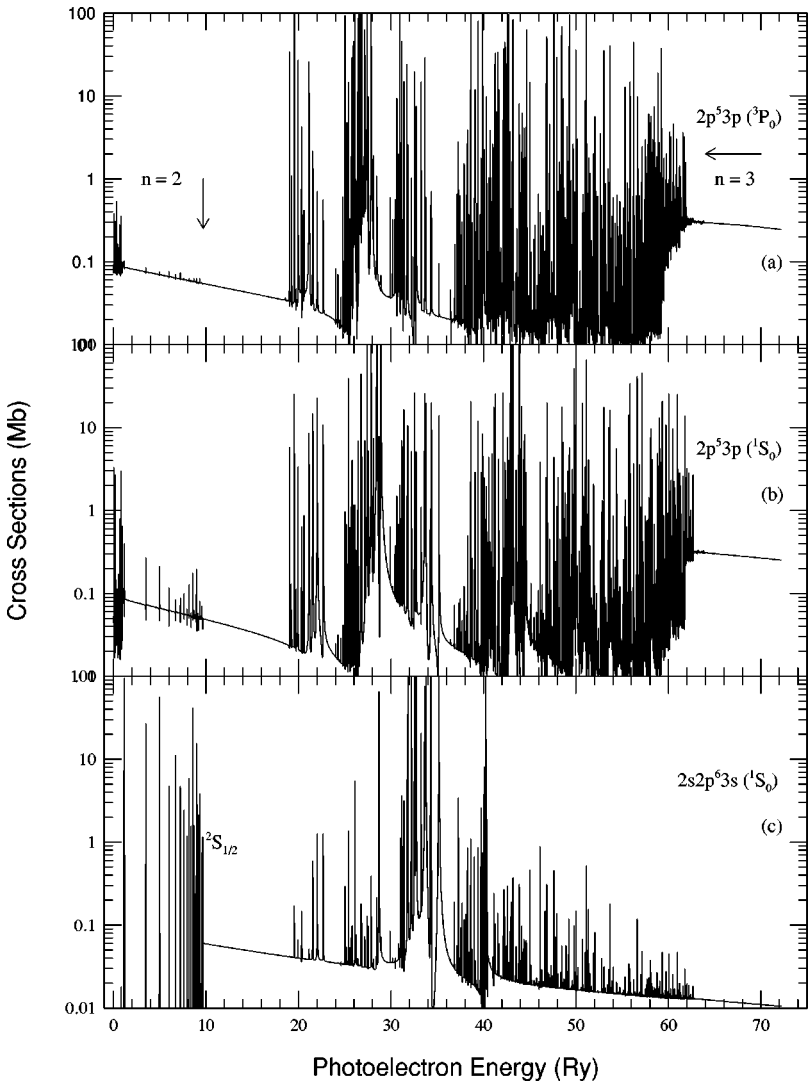

FIG. 3. The 60CC photoionization cross sections of the first three excited levels of the $J=0$, even parity symmetry, with extensive series of resonances converging on to the $n=3$ thresholds. The $n=2$ resonance strengths are much weaker.

range covered by the three-level calculations shown in Figs. 1 and 2, are much smaller than in the 60CC cross sections. This implies, in particular, that resonant recombination into the $n=3$ series of resonances converging on to a large number of excited states will be important for $e+$ion recombination, discussed in Sec. IV A 2.

As the above results show, the three-level calculations in the present and earlier works (e.g., [7,3]) are inadequate for the entire energy range of interest in practical applications for photoionization and recombination. Also, a three-level calculation gives little indication of the complexity of the cross sections, particularly for the excited states, since it covers only $\Delta n=0$ core excitations and couplings that are responsible for resonances. The $\Delta n>0$ couplings can be much stronger and give rise to more extensive resonances as in Fig. 3. It is clear that although Fe XVII is a highly charged ion the electron correlation effects are not weak in excited-state photoionization, or in the near-threshold region. Finally, Fe XVII is a closed-shell system where simpler approximations (e.g., Haque *et al.* [7]) can be readily applied without explicit consideration of detailed multiplet and fine structure that is more involved in open-shell systems. Thus photoionization of other highly charged ions may not be amenable to the approximations described in [7]. In fact the atomic structure of open-shell Fe ions isoelectronic with the third row of the Periodic Table present considerable difficulties owing to strong coupling effects up to several hundred fine-structure levels. Such is the case in a number of scattering calculations carried out under the Iron Project for open-shell Fe ions with extensive resonance structures [6].

2. Photoexcitation-of-core (PEC) resonances

Giant resonances manifest themselves at photon frequencies associated with strong dipole transitions in the core ion. These are a particularly important example of the coupling effects and are called photoexcitation-of-core (PEC) resonances (e.g., [26,27]). The PEC resonances have the following properties: (i) they are at the photon frequency of the dipole transition in the core, (ii) they are present in photoionization cross sections of the entire Rydberg series of bound levels of the $e+$ion system, (iii) their width and height are orders of magnitude larger than individual Rydberg resonances, and (iv) they are related to the inverse resonant recombination process DR (discussed in Sec. IV A 3).

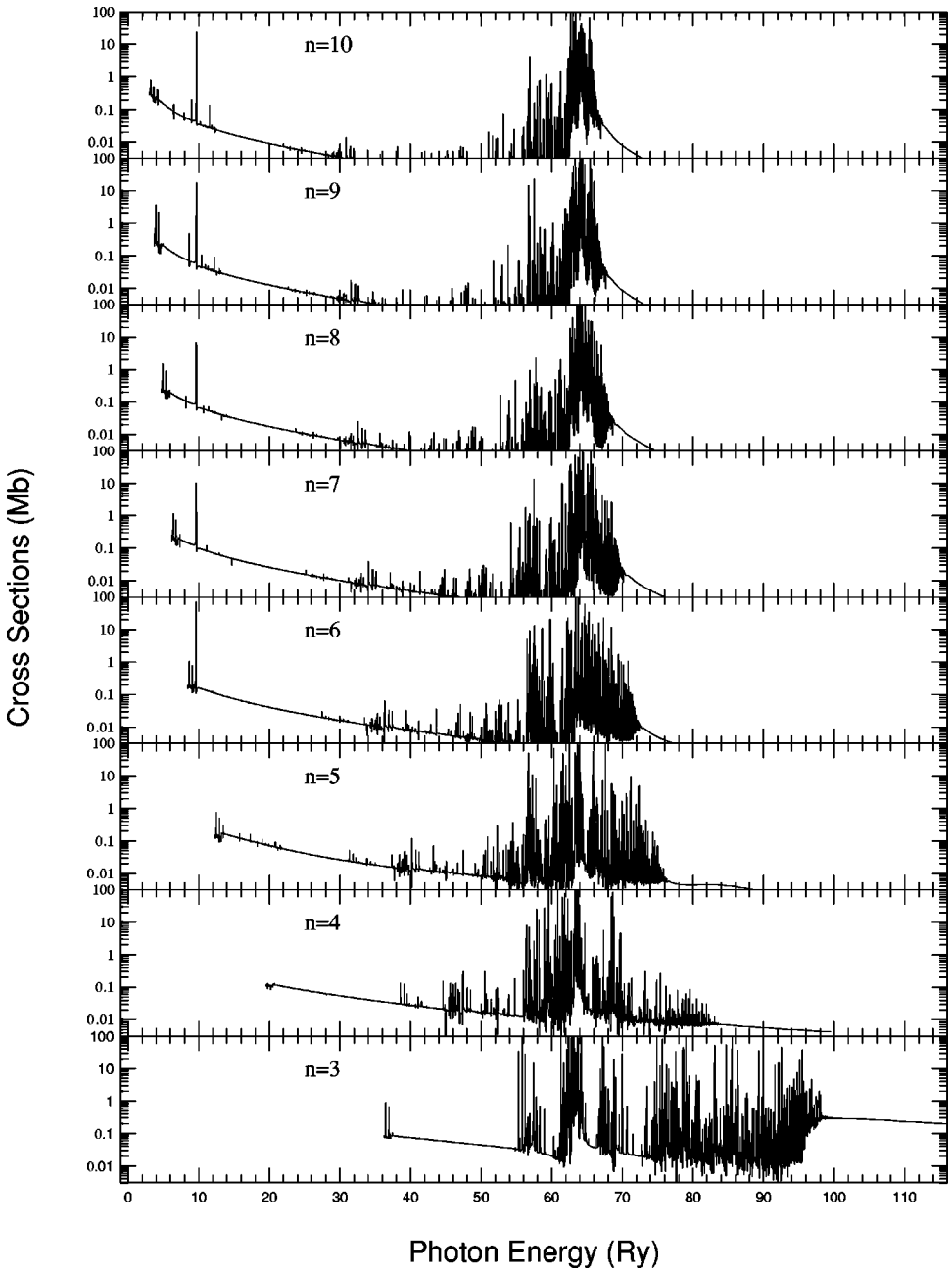

FIG. 4. Photoexcitation-of-core (PEC) resonances in photoionization of the $2p^5np(^3P_0)$ Rydberg series of levels of Fe XVII. The giant PEC resonance feature at approximately 63 Ry corresponds to strong dipole excitations in the transition arrays $2p^5$-$2p^43s,3d$ within the Fe XVIII core (60CC results).

The PEC features are most evident in photoionization cross sections, as a function of photon energy, of several members of a Rydberg series of bound levels where, in analogy with the DR process, the outer electron is weakly bound and may be considered a ''spectator,'' interacting but weakly with the core excitation(s). Figure 4 shows the large PEC feature in the 60CC photoionization cross sections of the series $2p^5np\ ^3P_0, n=3-10$ levels of Fe XVII. The PEC resonances in Fig. 4 are associated with not just one dipole transition, but several transitions belonging to the transition arrays $2p^5-2p^43s,3d$ at about 63 Ry corresponding to all such levels included in the 60CC expansion of the core-ion Fe XVIII [Eq. (1.1) and Table I)]. The PEC resonances rise an order of magnitude above the background, and are much wider than all other resonances. The different threshold ionization energies in Fig. 4 approach 0 as $n\rightarrow\infty$.

3. Radiation damping of autoionizing resonances

Radiation damping of resonances has been addressed in many previous works. It was pointed out in Ref. [25] that it is likely to be of practical importance only for H-like and He-like core ions, when the core radiative transition rates are of the same order as the autoionization rates, typically 10^{13-14} sec^{-1}, but not for other ionic systems. Fe XVII was explicitly mentioned in [25] as the next possible candidate (other than H-like and He-like ions) for an investigation of the radiation damping effects *in toto*. We discuss here the radiation damping involving the resonances associated with the $n=2$ levels in the context of low-energy recombination, and leave the discussion on the $n=3$ resonances in future when the much more extensive photorecombination calculations with the 60CC target are presented. It might be noted,

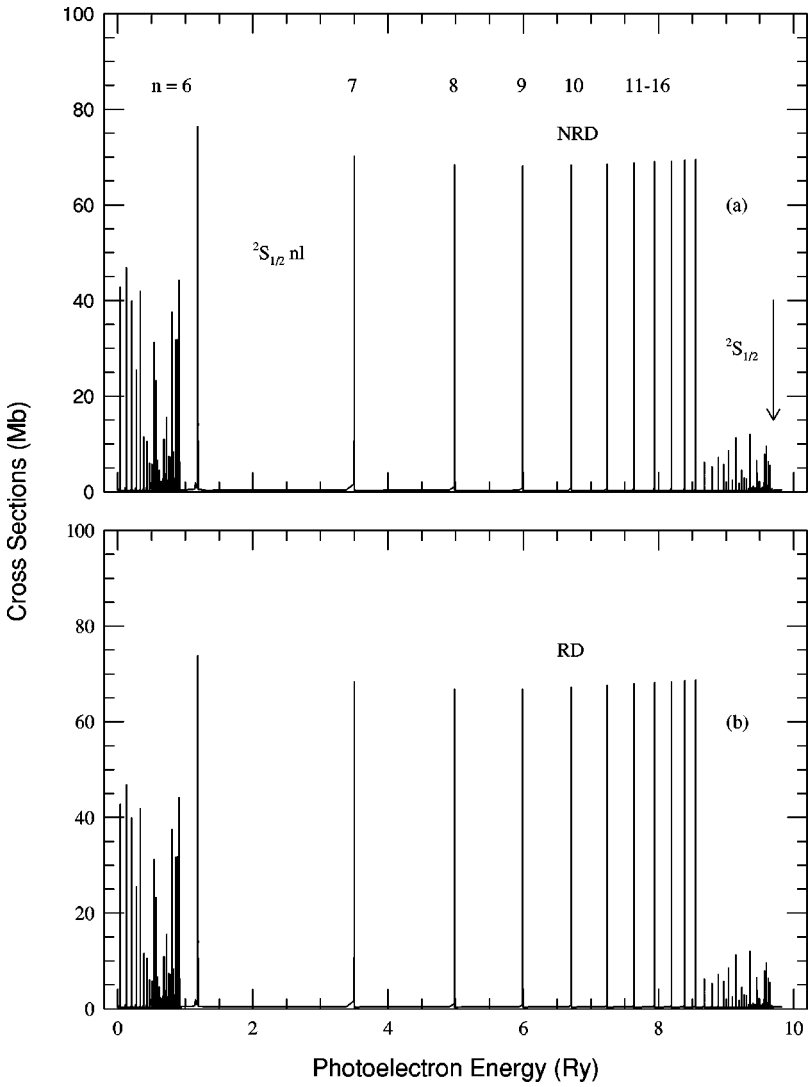

FIG. 5. Ground-level photoionization cross sections (a) without radiation damping (NRD) of resonances, and (b) with radiation damping (RD), showing a negligible effect up to the $n=16$ complex (higher n complexes are not resolved).

however, that although the radiative decay rates of the $n=3$ levels are higher, they also have additional autoionization modes of decay into excited $n=2$ levels.

The associated core transition rates in Fe XVIII for $2s^1 2p^6(^2S_{1/2})$ to $2s^2 2p^5(^2P^o_{3/2})$ and $2s^2 2p^5(^2P^o_{1/2})$ are 9.13×10^{10} and 3.31×10^{10} sec^{-1}, respectively. Figure 5 shows an enhanced view of the radiatively damped (RD) and undamped (NRD) resonances in photoionization of Fe XVII up to resonances complexes with $n=16$. The PR calculations in the unified formulation generally employ cross sections up to $n=10$ only. No significant effect is discernible between Figs. 5(a) and 5(b), and it is concluded that radiation damping of resonances in n complexes up to $n=10$ [e.g., group (a)] is not likely to affect any practical applications of the computed photoionization and recombination cross sections. That is not to say that resonances with sufficiently high n and l will not be damped significantly (or completely); since the autoionization rates decrease as n^{-3}, they must. However, such resonances are extremely narrow (not, for example, evident in Fig. 5), and do not affect effective photoionization or recombination cross sections. Therefore it is unlikely that radiation damping of group (a) resonances (an integral part of the unified $e+$ion recombination calculations) in any other ionic system up to the iron-peak elements will be important, since the dipole transition probabilities of resonance transitions in all ions up to Fe ions are less than or equal to those in Fe XVIII, of the order of 10^{12} sec^{-1}, with the already noted exception of H-like and He-like ions [25].

B. Electron-ion recombination

Salient features of the $e+$Fe XVIII$\rightarrow$Fe XVII recombination are described within the unified formulation, and with reference to experimental data from the ion storage ring at Heidelberg, Germany [28].

1. Comparison with experiment

Both the unified cross sections and experimental measurements naturally measure the combined nonresonant and resonant (RR and DR) contributions to $e+$ion recombination and should in principle be compared directly. Figure 6 from Ref. [8] shows a comparison of the present unified cross sections as computed in detail, and averaged over a Gaussian function for comparison with experiment, together with the experi-

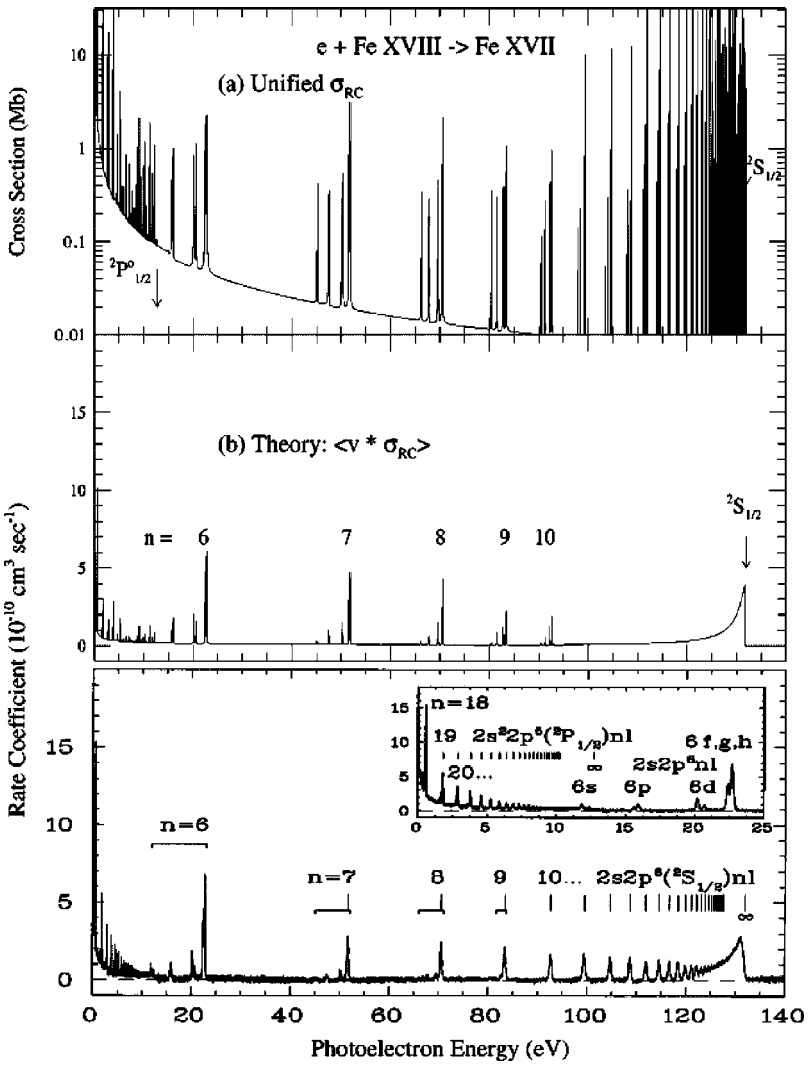

FIG. 6. Unified $e+$Fe XVIII$\rightarrow$Fe XVII recombination cross sections (upper panel) with detailed resonance complexes below the $n=2$ thresholds of Fe XVIII; Gaussian averaged over a 20-meV full width at half maximum (middle panel); experimental data from ion storage ring measurements [28] (bottom panel).

mental cross sections [28]. The agreement is generally very good over the entire range, and in both the detail and the magnitude of resonances. This includes the dominant DR contribution below the $^2S_{1/2}$ threshold connected via a dipole transition; in this range the background nonresonant contribution (RR) is small. On the other hand, the weaker series of resonances $^2P_{1/2}nl$ lie in the near-threshold region dominated by the nonresonant contribution that rises steeply as $E\rightarrow 0$, and is therefore not a major contributor to the $e+$ion recombination rate (discussed below). Thus the unified theoretical (and experimental) results shown in Fig. 6 display the three related, but discernible, types of contributions to total $e+$Fe XVIII$\rightarrow$Fe XVII recombination cross section: the overlapping nonresonant (RR) contribution and the DR contribution from the $^2P^o_{1/2}nl$ series, and the mainly DR contribution from the $^2S_{1/2}nl$ series.

2. Resonance strengths and rate coefficients

The experimental data in Fig. 6 do not precisely delineate or identify the resonances, and the background contribution (RR-type) is not ascertained from the measurements, possibly owing to a contribution from charge transfer recombination [28]. The blended resonance features in the experimental data are fitted to a beam response function to eliminate the background, and their energies are determined approximately according to n and l, using nonrelativistic l-dependent quantum defects in the Rydberg formula. However, l is not a good quantum number and the number of l resonances within an n-complex is not exactly known. The theoretical resonances on the other hand are uniquely identified with the intermediate coupling spectroscopic designation $(S_iL_iJ_i)nlJ\pi$. Therefore a 1–1 correspondence between the experimental measurements and relativistic cross sections cannot be established. Further, since the background contribution, although dominant at low energies as $E\rightarrow 0$ (Fig. 6), is not considered, a direct comparison with the unified cross sections and the experimental data [28] is not possible.

Nonetheless, for n-complexes where the background contribution is small compared to the resonant part, we may compare the average ''resonance strengths'' [28], although these are not exactly defined (see [29] for a definition of the resonance oscillator strength in terms of the integrated $df/d\epsilon$, the differential oscillator strength per unit energy). Figures 7(b)–7(d) show a detailed view at high resolution of the first three $^2S_{1/2}nl[J]$ complexes, with $n=6,7,8$. In order

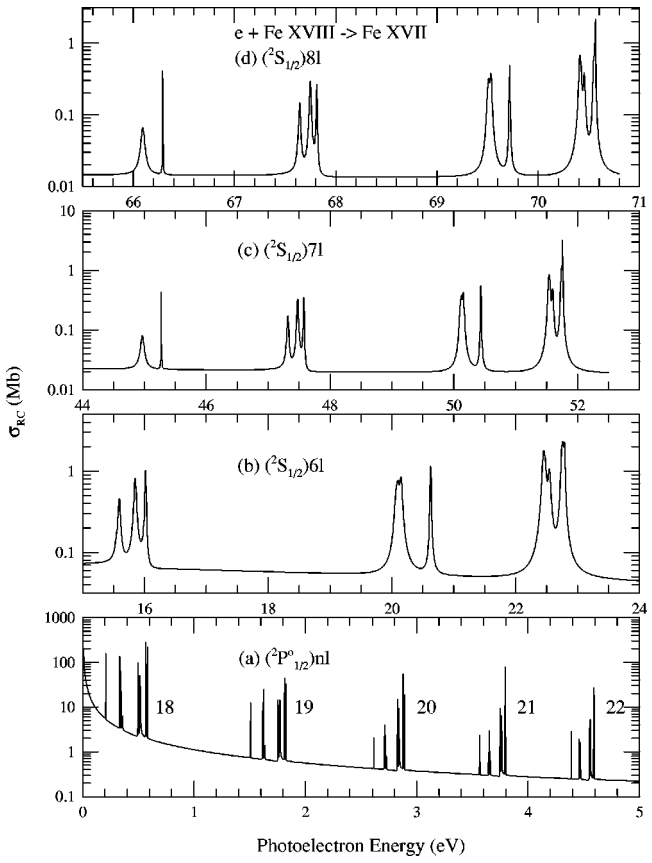

FIG. 7. Resolved resonance complexes $(S_iL_iJ_inlJ\pi)$ in the unified recombination cross sections: (a) $^2P^o_{1/2}nl$, (b) $^2S_{1/2}6l$, (c) $^2S_{1/2}7l$, (d) $^2S_{1/2}8l$. The lowest resonance group in the $n=6$ complex lies below the $^2P^o_{1/2}$ threshold among high-n $^2P^o_{1/2}nl$ resonances and is not shown. The complexity of resonance structures is barely apparent from (a), and even less so from the experimental data in Fig. 6 (lowest panel); 2985 resonances have been resolved in the 0–5-eV range shown in (a).

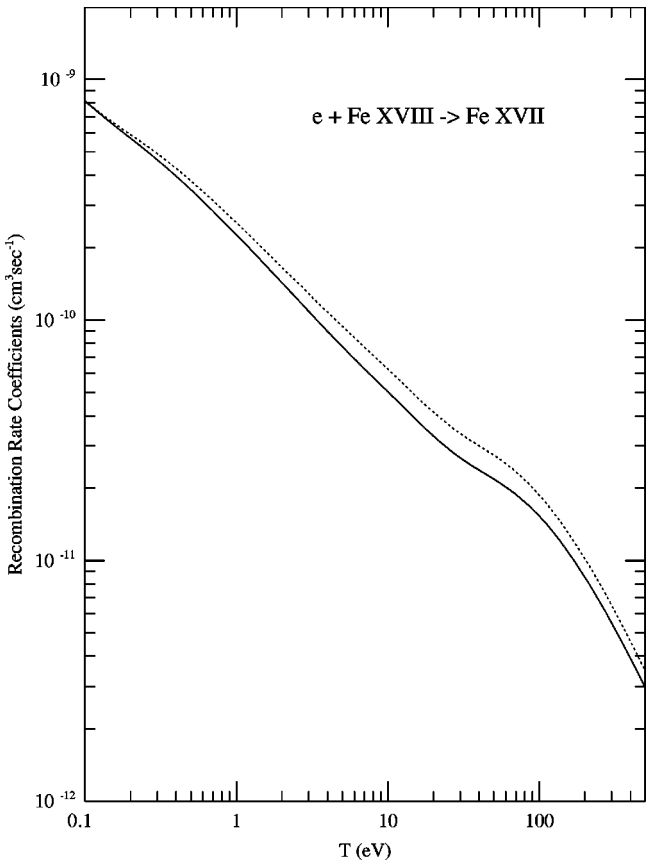

FIG. 8. Unified recombination rate coefficient $\alpha_R(T)$ (solid line) with σ_{RC} including only the $n=2$ resonances (as in the experimental data [28]), and the sum of the experimental DR rate coefficient + nonresonant background (RR-type) contribution extracted from the present calculations (dashed line). The maximum difference is $\sim 20\%$.

to ensure complete resolution of resonances an energy mesh of up to 10^{-7} eV was used before numerical integration. The integrated, and summed, resonance strengths for the $n=6,7,8$ complexes are 1201.2, 421.8, and 221.1 cm^2 eV, compared to experimental values of 1240.2, 412.0, and 253.9 [28]. The present value for $n=7$ complex is higher than reported in Ref. [8] as it is recalculated with higher resolution. The value for the $n=8$ complex has been complemented by the contributions from $J>7$ symmetries, $J\pi=8^o$ and 9^e; without which the value is 200.5 cm^2 eV. Although the theoretical resonance strengths were checked to have converged with respect to the energy mesh, they seem to be somewhat systematically lower than the reported experimental data (the theoretical MCBP and the MCDF values in [28] also showed the same trend).

Figure 7(a) is rather different in that it shows the much narrower $^2P^o_{1/2}nl$ resonances with high $n=18-22$. While it is not apparent from the figure, nor from the experimental data in Fig. 6 (bottom most panel), there are 2985 resonances found in the small 0–5-eV range just above the ionization threshold of Fe XVII. The number of resonances reflects the large number of high-n near-degenerate resonances $(\sim 2n^2)$ converging on to the various series limits. The set of (E_o,Γ_a,Γ_r) for all these resonances have been computed. The integrated resonance strengths for the $n=18$, 19, and 20 complexes are 2290.9, 521.6, 290.1 cm^2 eV, compared to experimental values [28] of 2452.8, 605.7, and 336.5, respectively. Again, we find the integrated values to be up to about 10% lower than measured, although here the uncertainties are greater than for the lower-n $^2S_{1/2}nl$ resonances in Figs. 7(b)–7(d), since they may not have been completely resolved and because the integration energy ranges are very closely spaced. Also, the precise range of angular momenta (l,J) in the ion storage rings is not known [28] and $J\leqslant 7$ may not be quite sufficient for better agreement. A detailed comparison of resonances beyond this level is neither feasible nor necessary at this time. Although not all resonances are experimentally identified, the theoretical cross sections, resonance strengths, and rates (see below) can be compared, as shown, to within experimental and theoretical uncertainties.

Finally we evaluate quantities of practical interest, the Maxwellian-averaged unified $e+$ion recombination rate coefficients $\alpha_R(T)$ shown in Fig. 8. These are compared with

TABLE III. Comparison of the present energies and the NIST values (Ry) for selected fine-structure levels of Fe XVII.

Level	Present	NIST
$2s^2 2p^6\ ^1S_0$	0.0000	0.0000
$2s^2 2p^5 3p\ ^3P_0$	56.6532	56.5155
$2s^2 2p^5 3p\ ^1S_0$	58.0986	57.8897
$2s^2 2p^5 3s\ ^1P_1^o$	53.5708	53.4300
$2s^2 2p^5 3s\ ^3P_1^o$	54.4475	54.3139
$2s^2 2p^5 3d\ ^3P_1^o$	59.1231	58.9810
$2s^2 2p^5 3d\ ^3D_1^o$	59.8763	59.7080
$2s^2 2p^5 3d\ ^1P_1^o$	60.8849	60.6000
$2s 2p^6 3p\ ^1P_1^o$	65.7990	65.6010
$2s 2p^6 3p\ ^3P_1^o$	66.1216	65.9230
$2s^2 2p^5 4s\ ^1P_1^o$	72.0294	71.8600
$2s^2 2p^5 4s\ ^3P_1^o$	72.9394	72.7400
$2s^2 2p^5 4d\ ^3P_1^o$	74.1757	73.9400
$2s^2 2p^5 4d\ ^3D_1^o$	74.4979	74.3000
$2s^2 2p^5 4d\ ^1P_1^o$	75.3539	75.1700

the sum of the available experimental DR rate coefficients [28], and the background RR-type contribution extracted from the present theoretical cross sections. The agreement is of the order of 20%, the estimated uncertainty in both the experimental and theoretical datasets. However, we believe that the agreement could be slightly better since the theoretical results might be somewhat enhanced if the few $J\pi$ symmetries with $J>7$, for resonances with $n\leqslant 10$, are also included. These were omitted to reduce the complexity of calculations (except to gauge their effect on the completeness of the $n=8$ complex mentioned above), and since their resonant contribution is small.

3. $\Delta n=1$ resonances and high-energy recombination

Thus far only the low-energy $\Delta n=0$ resonances due to the $n=2$ levels of Fe XVIII have been considered. However, as demonstrated in this work, the high-energy recombination cross sections due to the $n=3$ levels are much larger and will be more important at high temperatures close to the temperature of maximum abundance of Fe XVII in collisional equilibrium, around $T=4-5\times 10^6$ K. This would especially be the case owing to the huge PEC resonances shown in Fig. 4 that in fact correspond to the peak values of DR due to resonances converging on to the series limits of strong dipole $\Delta n=1$ transitions. Therefore, in addition to the DR bump corresponding to the $n=2$ resonances in the total $\alpha_R(T)$ shown in Fig. 8, we expect a much larger bump at higher temperatures from the $n=3$ resonances. However, the 60CC calculations are orders of magnitude more expensive in terms of computational and other resources and, although they are in progress, would require a considerable amount of time to be completed.

C. Bound states and transition probabilities of Fe XVII

In addition to photoionization and recombination the BPRM calculations also enable unprecedented quantities of accurate bound-state and transition probability datasets in intermediate coupling (e.g., [30]). The accuracy of these results is comparable to the most elaborate configuration-interaction atomic structure calculations since the wave function in Eq. (2.1) entails a large configuration expansion, with each channel as a bound configuration of the $e+$ion system for $E<0$ and symmetry $J\pi$. These calculations are in progress for all fine-structure levels of Fe XVII up to $n=10$, and associated $E1$ A and f values. Table III provides a brief sample of the bound-level energies computed for some of the levels of interest in this work. Together with the electron-impact excitation collision strengths for Fe XVII in progress [31], these results should help complete the radiative and collisional data for Fe XVII needed for most plasma modeling applications.

V. CONCLUSION

The most extensive relativistic close-coupling calculations for photoionization and recombination of an atomic species are reported for the astrophysically important ion Fe XVII. Based on this work we may note the following conclusions: (i) self-consistent datasets may be obtained for photoionization and recombination within the close-coupling formulation, (ii) the coupling to the $n=3$ thresholds strongly manifests itself in excited-state photoionization; resonances enhance the effective cross sections by orders of magnitude particularly below thresholds coupled via dipole photoexcitation-of-core levels, (iii) unified $e+$ion recombination cross sections are in good agreement with experimental data in terms of both detailed resonance strengths and rates; the resonances have been delineated at very high resolution with considerably more structure than experimentally observed (in principle all quantum-mechanically allowed resonances in intermediate coupling may be obtained), (iv) it is necessary to consider the higher $n=3$ levels in high-energy recombination that would dominate the DR part of the $e+\text{Fe XVIII}\rightarrow\text{Fe XVII}$ recombination at temperatures close to maximum abundance of Fe XVII in coronal (collisional) equilibrium, and (v) it is necessary to account for not only relativistic fine structure but also the strong coupling among those levels in order to accurately reproduce the results for photoionization and recombination over the entire range of practical interest.

ACKNOWLEDGMENTS

We would like to thank Dr. Werner Eissner for several contributions and Mr. Guoxin Chen for assistance with the calculations. This work was supported in part by the NSF and NASA. The computational work was carried out at the Ohio Supercomputer Center in Columbus, Ohio.

[1] J.K. Laming *et al.*, Astrophys. J. Lett. **545**, L161 (2000).
[2] A.K. Bhatia and S.O. Kastner, Astrophys. J. **516**, 482 (1999).
[3] M. Mohan, M. Le Dourneuf, A. Hibbert, and P.G. Burke, Phys. Rev. A **57**, 3489 (1998).
[4] D.G. Hummer, K.A. Berrington, W. Eissner, A.K. Pradhan, H.E. Saraph, and J.A. Tully, Astron. Astrophys. **279**, 298 (1993).
[5] M.J. Seaton, Y. Yu, D. Mihalas, and A.K. Pradhan, Mon. Not. R. Astron. Soc. **266**, 805 (1994).
[6] Information on the Iron Project and publications may be presently found at the following homepages: www.usm.uni-muenchen.de/people/ip/iron-project.html and www.astronomy.ohio-state.edu/~pradhan.
[7] N. Haque, H.S. Chakraborty, P.C. Deshmukh, S.T. Manson, A.Z. Meszane, N.C. Deb, Z. Felfli, and T.W. Gorczyca, Phys. Rev. A **60**, 4577 (1999).
[8] A.K. Pradhan, S.N. Nahar, and H.L. Zhang, Astrophys. J. Lett. **549**, L265 (2001).
[9] T. Kallman, in *Atomic Processes in Plasmas* (AIP Press, New York, 1995).
[10] M. Arnaud and J. Raymond, Astrophys. J. **398**, 394 (1992).
[11] S.N. Nahar and A.K. Pradhan, Phys. Rev. A **49**, 1816 (1994).
[12] R.H. Bell and M.J. Seaton, J. Phys. B **18**, 1589 (1985).
[13] H.L. Zhang, S.N. Nahar, and A.K. Pradhan, J. Phys. B **32**, 1459 (1999).
[14] H.L. Zhang and A.K. Pradhan, Phys. Rev. Lett. **78**, 195 (1997).
[15] S.N. Nahar, A.K. Pradhan, and H.L. Zhang, Astrophys. J., Suppl. Ser. **131**, 375 (2000).
[16] S.N. Nahar, A.K. Pradhan, and H.L. Zhang, Astrophys. J. Suppl. Ser. (to be published).
[17] P.G. Burke, A. Hibert, and D. Robb, J. Phys. B **4**, 153 (1971).
[18] K.A. Berrington, P.G. Burke, K. Butler, M.J. Seaton, P.J. Storey, K.T. Taylor, and Yu. Yan, J. Phys. B **20**, 6379 (1987).
[19] N.S. Scott and K.T. Taylor, Comput. Phys. Commun. **25**, 347 (1982).
[20] K.A. Berrington, W.B. Eissner, P.H. Norrington, Comput. Phys. Commun. **92**, 290 (1995).
[21] W. Eissner, M. Jones, and N. Nussbaumer, Comput. Phys. Commun. **8**, 270 (1974).
[22] J. Sugar and C. Corliss, in *Atomic Energy Levels of the Iron-Period Elements: Potassium through Nickel*, special issue of J. Phys. Chem. Ref. Data (1985); the Fe XVIII data are from U. Feldman, G.A. Doschek, R.D. Cowan, and L. Cohen, J. Opt. Soc. Am. **63**, 1445 (1973).
[23] J.R. Fuhr, G.A. Martin, and W.L. Wiese, *Atomic Transition Probabilities*, special issue of J. Chem. Phys. Ref. Data **17**, 1 (1988); the data are calculated by K.T. Cheng, Y.-K. Kim, and J.P. Desclaux, At. Data Nucl. Data Tables **24**, 1111 (1979) and B.C. Fawcett, *ibid.*, **31**, 495 (1984).
[24] H.L. Zhang, Phys. Rev. A **57**, 2640 (1998).
[25] A.K. Pradhan and H.L. Zhang, J. Phys. B **30**, L571 (1997).
[26] Y. Yu and M.J. Seaton, J. Phys. B **20**, 6409 (1987).
[27] S.N. Nahar and A.K. Pradhan, Phys. Rev. A **44**, 2935 (1991).
[28] D. W. Savin *et al.*, Astrophys. J., Suppl. Ser. **123**, 687 (1999).
[29] A.K. Pradhan, Astrophys. J. Lett. **545**, L165 (2000).
[30] S.N. Nahar and A.K. Pradhan, Astron. Astrophys., Suppl. Ser. **135**, 347 (1999).
[31] G.X. Chen and A.K. Pradhan (unpublished).